

One-loop diagrams in nucleon-nucleon scattering

M. J. Zuilhof and J. A. Tjon

Institute for Theoretical Physics, University of Utrecht, Princetonplein 5, 3508 TA Utrecht, The Netherlands

(Received 22 December 1981)

Within the framework of the Blankenbeckler-Sugar equations the effects of one-loop corrections to the driving force are studied in the two-nucleon system. In particular, contributions from the direct and crossed box two-pion exchange diagrams are calculated. An analysis is made at the one-loop level for both pseudoscalar and pseudovector pion-nucleon coupling using a geometric unitarization. In a model with one boson exchanges it is shown that the agreement between the Bethe-Salpeter and the quasipotential results does not improve in all partial waves when the one-loop contributions are included. Various qualitative fits to the experimental data are presented for such a model.

NUCLEAR REACTIONS NN system, quasipotential equations compared with the Bethe-Salpeter equations. Method to calculate one-loop contributions. Comparison of pseudovector and pseudoscalar pion-nucleon coupling at the one-loop level.

I. INTRODUCTION

In the search for approximations to the Bethe-Salpeter equation (BSE) one is led to consider quasipotential equations (QPE), which have mathematically a more simple structure. In a previous paper¹ we gave a brief summary of this approach, and examined the effects of correction terms for the case of the Gross approximation.² In this paper we extend our studies to the case of the Blankenbeckler-Sugar (BbS) approximation, where it is possible, in contrast to the Gross approximation, to include the contributions of the crossed-box diagrams without essential difficulties.

Historically the pion-nucleon coupling is assumed to be of the pseudoscalar (PS) type,

$$\mathcal{L}_{\pi NN}^{\text{PS}} = ig_{\text{PS}} \bar{\psi} \gamma_5 \vec{\tau} \psi \cdot \vec{\phi}. \quad (1.1)$$

The main reason for this choice is the fact that a theory with this type of coupling is renormalizable. The other choice,

$$\mathcal{L}_{\pi NN}^{\text{PV}} = g_{\text{PV}} \bar{\psi} \gamma_5 \gamma_\mu \vec{\tau} \psi \cdot \partial^\mu \vec{\phi}, \quad (1.2)$$

necessitates the introduction of a cutoff in momentum space. However, since the basic underlying theory may be in terms of more fundamental fields, one might consider these pion-nucleon couplings as phenomenological representations of an effective in-

teraction thereby making the argument of renormalizability less essential. Analysis of pion electroproduction and photoproduction experiments³ as well as calculations of the nucleon-nucleon phaseshifts with the BSE (Ref. 4) indicate that pseudovector (PV) coupling, Eq. (1.2), might be preferred above PS coupling. Some aspects of this problem are considered here within the QPE approach using the BbS equation.

In particular, the effects of the two-pion-exchange (TPE) processes are discussed for both PV and PS pion-nucleon coupling. These TPE contributions play an important role in the description of the nuclear force at intermediate distances. In studies of the BSE with one-boson exchange (OBE) it was found⁴ that the negative-energy contributions in a PS theory lead to extremely strong effects in the lower partial waves. Possible cancellations of these contributions by the crossed TPE diagram are examined here in detail. In general we find that this compensation does not take place in all partial waves.

The organization of the paper is as follows. In Sec. II we briefly introduce the BbS approximation for particles with spin. Our treatment differs slightly from previous calculations^{5,6} in the sense that we also allow for negative-energy spin components in the intermediate states. To study the

TPE effects we need to compute one-loop diagrams. In Sec. III we describe a way to evaluate the direct and the crossed-box diagrams for nucleon-nucleon scattering. The effects of the TPE processes are discussed in Sec. IV at the one-loop level using geometric unitarization. We find that the box diagram contributions are badly approximated in the quasipotential approach, as are the negative-energy intermediate states. The latter result is confirmed in Sec. V where the BbS equation is compared to the BSE, with and without negative-energy states. Section VI is devoted to a description of a number of qualitative fits of the BbS phaseshifts to the experimental data with the corrections from the direct and crossed box contributions included. In the last section we make some concluding remarks and we note some essential difficulties in calculating the

electromagnetic properties of the two-nucleon system within the BbS approach.

II. THE BbS APPROXIMATION

The form of the BbS equation is taken to be slightly different from the one usually used. The procedure followed by Partovi and Lomon⁵ is to truncate the Bethe-Salpeter equation by neglecting the negative-energy states and to approximate the positive-energy BS propagator by a quasipotential propagator. In our approach it is not necessary to drop the negative-energy states. We write the BS propagator for two spin $\frac{1}{2}$ particles as the product of the propagator for two scalar particles and a two-particle spinor operator:

$$\left[\frac{P^{(1)}}{2} + \not{p}^{(1)} - m \right]^{-1} \left[\frac{P^{(2)}}{2} - \not{p}^{(2)} - m \right]^{-1} = \left[\frac{P}{2} + \not{p} + m \right]^{(1)} \left[\frac{P}{2} - \not{p} + m \right]^{(2)} \times \left[\left[\frac{P}{2} + p \right]^2 - m^2 + i\epsilon \right]^{-1} \left[\left[\frac{P}{2} - p \right]^2 - m^2 + i\epsilon \right]^{-1}. \quad (2.1)$$

Here P is the total and p the relative momentum of the two nucleons with equal mass m . The scalar propagator is then replaced by a dispersion integral

$$2\pi i \int_{4m^2}^{\infty} \frac{ds'}{s' - s - i\epsilon} f(s', s) \delta^{(+)} \left[\left[\frac{P'}{2} + p \right]^2 - m^2 \right] \delta^{(+)} \left[\left[\frac{P'}{2} - p \right]^2 - m^2 \right], \quad (2.2)$$

where $\delta^{(+)}$ means that only the positive energy root of the argument is to be included. In Eq. (2.2), $S = P^2 = 4E^2$ and $P' = \sqrt{s'}/sP$. To reproduce the two-particle unitarity condition the otherwise arbitrary function f must be unity when s' equals s . Following Ref. 6 we make the special choice

$$f(s', s) = \frac{2\sqrt{s'}}{\sqrt{s'} + \sqrt{s}}. \quad (2.3)$$

As a result we get for the BbS propagator for particles with spin

$$g(p_0, p) = \left[(E + E_p) \Lambda_+ + (E - E_p) \Lambda_- \right]^{(1)} \times \left[(E + E_p) \Lambda_+ + (E - E_p) \Lambda_- \right]^{(2)} \times \frac{i\pi\delta(p_0)}{(E + E_p)^2 (E_p - E - i\epsilon)}, \quad (2.4)$$

where Λ_{\pm} is defined in terms of the helicity spinors defined in Ref. 7:

$$\Lambda_+ = \sum_{\lambda} U_{\lambda} \bar{U}_{\lambda},$$

$$\Lambda_- = \sum_{\lambda} W_{\lambda} \bar{W}_{\lambda}. \quad (2.5)$$

Introducing the energy-spin states $+$, $-$, e , and o ,⁸ we find that the propagator is diagonal in this representation:

$$g_{++}(p_0, p) = i\pi\delta(p_0) \frac{1}{E_p - E - i\epsilon},$$

$$g_{--}(p_0, p) = i\pi\delta(p_0) \frac{E_p - E}{(E_p + E)^2}, \quad (2.6)$$

$$g_{ee}(p_0, p) = g_{oo}(p_0, p) = -i\pi\delta(p_0) \frac{1}{E_p + E},$$

and all other elements are zero.

The effect of the BbS approximation is that all states that are odd in the relative energy⁸ are eliminated. For $J \neq 0$ we are left with six channels in the case of the coupled triplet states and with four channels in the case of the singlet and coupled triplet states:

$$\begin{aligned}
&\text{coupled triplet: } {}^3(J-1)_J^+, {}^3(J+1)_J^+, {}^3(J-1)_J^-, {}^3(J+1)_J^-, {}^1J_J^e, {}^3J_J^e, \\
&\text{uncoupled triplet: } {}^3J_J^+, {}^3J_J^-, {}^3(J-1)_J^e, {}^3(J+1)_J^e, \\
&\text{singlet: } {}^1J_J^+, {}^1J_J^-, {}^3(J-1)_J^e, {}^3(J+1)_J^e.
\end{aligned} \tag{2.7}$$

For $J=0$ the states with $L=J-1$ or with $S=1$ and $L=J$ are absent, so that we have

$$\begin{aligned}
&\text{coupled triplet: } {}^3P_0^+, {}^3P_0^-, {}^1S_0^e, \\
&\text{singlet: } {}^1S_0^+, {}^1S_0^-, {}^3P_0^e.
\end{aligned} \tag{2.8}$$

As in Ref. 1 we use the term two-channel approximation when we ignore the channels containing negative-energy states. The case with all channels included will generically be called the six-channel calculation. The solution of the resulting equations is obtained in the same way as described in Sec. II of Ref. 1.

III. EVALUATION OF THE TWO-BOSON-EXCHANGE DIAGRAM

In the analysis of the two-boson-exchange effects it is necessary to evaluate the matrix elements of the direct and the crossed box diagrams between partial wave states. In this section the procedure is described and a simple example is treated in detail. The method is based on the treatment of general four-point functions at the one-loop level described

$$\begin{aligned}
D_{2\mu,\nu} &= -i \int d^4k k_\mu k_\nu D \\
&= v_{1,\mu} v_{1,\nu} D_{21} + v_{2,\mu} v_{2,\nu} D_{22} + v_{3,\mu} v_{3,\nu} D_{23} + \left\{ v_{1,\mu}, v_{2,\nu} \right\} D_{24} + \left\{ v_{1,\mu}, v_{3,\nu} \right\} D_{25} \\
&\quad + \left\{ v_{2,\mu}, v_{3,\nu} \right\} D_{26} - g_{\mu\nu} D_{27},
\end{aligned} \tag{3.4}$$

where $\{a_\mu, b_\nu\} = a_\mu b_\nu + a_\nu b_\mu$. In our work we do not need the higher moments. The numerical values of the form factors D_{11}, D_{12}, \dots can be obtained from the program FORMF written by Veltman.¹⁰

We now turn to the evaluation of the box diagrams used in our calculation. As an example of our procedure we will work out explicitly the expressions for the crossed box of pions, whereby the pion-nucleon interaction is given by the PS coupling.

The momenta are chosen as shown in Fig. 2. The contribution of this diagram is

in Ref. 9. For convenience we repeat here the essential steps of this treatment. Consider a four-point function with external momenta v_i , internal masses m_i , and a loop-momentum k , as defined in Fig. 1. The product of the propagators of the internal particles is abbreviated as

$$\begin{aligned}
D &= \frac{1}{k^2 - m_1^2} \frac{1}{(k + v_1)^2 - m_2^2} \frac{1}{(k + v_1 + v_2)^2 - m_3^2} \\
&\quad \times \frac{1}{(k + v_1 + v_2 + v_3)^2 - m_4^2}.
\end{aligned} \tag{3.1}$$

The scalar four-point function

$$D_0 = -i \int d^4k D \tag{3.2}$$

is a Lorentz-invariant function of the external momenta and the internal masses (which are assumed to have an infinitesimal negative imaginary part). The higher moments of the four-point function can also be written in terms of scalar form factors, for example, we can write the first and the second moment as

$$\begin{aligned}
D_{1\mu} &= -i \int d^4k k_\mu D \\
&= v_{1,\mu} D_{11} + v_{2,\mu} D_{12} + v_{3,\mu} D_{13},
\end{aligned} \tag{3.3}$$

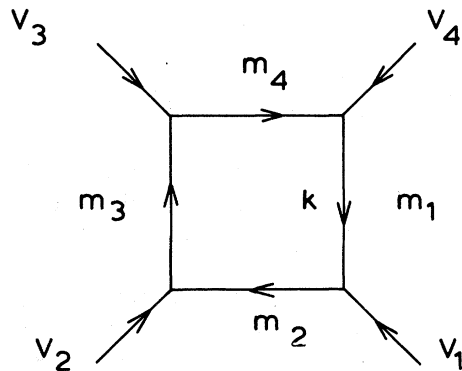


FIG. 1. Definition of the external momenta, the internal masses, and the loop momentum of the one-loop four point function.

$$X = -i\alpha \int d^4k \left[\gamma_5(k + Q_1 + m)\gamma_5 \right]^{(1)} \times \left[\gamma_5(k + P_2 + m)\gamma_5 \right]^{(2)} D, \quad (3.5)$$

where D is the product of the scalar parts of the pion and the nucleon propagators

$$D = \frac{1}{k^2 - \mu^2} \frac{1}{(k + P_2)^2 - m^2} \frac{1}{(k + P_2 - Q_2)^2 - \mu^2} \times \frac{1}{(k + Q_1)^2 - m^2}. \quad (3.6)$$

The factor α contains the coupling parameters, the factors from the Feynman rules, and the isospin operators

$$\alpha = \frac{1}{4\pi^3} \left[\frac{g_{\text{ps}}}{4\pi} \right]^2 \tau_i^{(1)} \tau_j^{(1)} \tau_j^{(2)} \tau_i^{(2)}. \quad (3.7)$$

The isospin operators contribute a factor of -3 in an isospin zero state and a factor of 5 in an isospin one state, which can be found immediately from the fact that

$$\tau_i^{(1)} \tau_j^{(1)} \tau_j^{(2)} \tau_i^{(2)} = 4\vec{I}^2 - 3, \quad (3.8)$$

where \vec{I} is the total isospin operator.

The connection between the crossed box considered here and the general four-point function of Fig. 1 is given by the following substitution

$$v_1 = P_2, \quad v_2 = -Q_2, \quad v_3 = P_1, \quad v_4 = -Q_1, \quad (3.9)$$

$$m_1 = \mu, \quad m_2 = m, \quad m_3 = \mu, \quad m_4 = m.$$

$$\begin{aligned} 0_1 &= 1^{(1)} 1^{(2)}, & 0_2 &= \gamma_0^{(1)} 1^{(2)}, & 0_3 &= 1^{(1)} \gamma_0^{(2)}, & 0_4 &= \gamma_0^{(1)} \gamma_0^{(2)}, \\ 0_5 &= \gamma_\mu^{(1)} \gamma^\mu{}^{(2)}, & 0_6 &= \gamma_0^{(1)} 0_5, & 0_7 &= 0_5 \gamma_0^{(2)}, & 0_8 &= \gamma_0^{(1)} 0_5 \gamma_0^{(2)}, \\ 0_9 &= \gamma_5^{(1)} \gamma_5^{(2)}, & 0_{10} &= \gamma_0^{(1)} 0_9, & 0_{11} &= 0_9 \gamma_0^{(2)}, & 0_{12} &= \gamma_0^{(1)} 0_9 \gamma_0^{(2)}, \\ 0_{13} &= \gamma_5^{(1)} 0_5 \gamma_5^{(2)}, & 0_{14} &= \sigma_{\mu\nu}^{(1)} \sigma^{\mu\nu}{}^{(2)}, & 0_{15} &= \gamma_0^{(1)} 0_{14}, & 0_{16} &= 0_{14} \gamma_0^{(2)}. \end{aligned} \quad (3.14)$$

Parity conservation requires that $\gamma_5^{(1)}$ always combines with $\gamma_5^{(2)}$. The operators are linearly independent, but they do not form an orthogonal basis, since 0_{14} contains 0_1 and 0_8 . Applying the above procedure to the operators listed in the second column of Table I we readily find that only the first five operators in (3.14) are needed for the simple example considered here. The explicit results are given in the third column of Table I. With the above reduction Eq. (3.10) assumes the form

$$X = \sum_n c_n 0_n, \quad (3.15)$$

The expression for the crossed box is now written in terms of $D0$, $D1$, and $D2$:

$$X = AD0 + B^\mu D1_\mu + C^{\mu\nu} D2_{\mu\nu}. \quad (3.10)$$

The operators A , B , and C are found by comparison with (3.5):

$$\begin{aligned} A &= \alpha(Q_1 - m)^{(1)}(P_2 - m)^{(2)}, \\ B_\mu &= \alpha\gamma_\mu^{(1)}(P_2 - m)^{(2)} + \alpha(Q_1 - m)^{(1)}\gamma_\mu^{(2)}, \\ C_{\mu\nu} &= \alpha\gamma_\mu^{(1)}\gamma_\nu^{(2)}. \end{aligned} \quad (3.11)$$

After substitution of (3.3) and (3.4) into (3.10) we obtain an expression in terms of the scalar form factors multiplied by operators which depend only on the external momenta. The operators multiplying the form factors are listed in the first column of Table I.

Next we evaluate, in the center of mass frame, the matrix elements of the box diagram between two-particle helicity states defined in Appendix B of Ref. 7. The two-particle states are direct products of one-particle helicity spinors U_λ^\pm which satisfy the (off-mass-shell) Dirac equation

$$\not{p} U_\lambda^\pm(\vec{p}) = \left[m + \gamma^0(p_0 \mp E_p) \right] U_\lambda^\pm(\vec{p}), \quad (3.12)$$

where

$$p = (p_0, \vec{p}) \text{ and } E_p = \sqrt{m^2 + \vec{p}^2}. \quad (3.13)$$

The upper index \pm labels the positive and negative-energy solutions. With (3.12) we can rewrite any box diagram encountered in our calculations in terms of the sixteen effective operators:

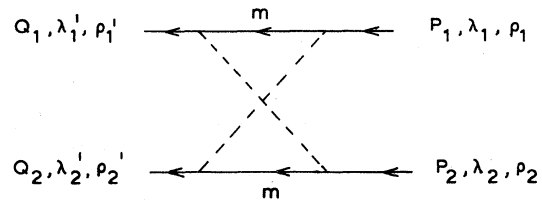


FIG. 2. The crossed box with external momenta P and Q , helicities λ , and energy-spin ρ . The pion mass is μ and m is the nucleon mass.

TABLE I. The operators and effective operators corresponding to the various form factors of the crossed box diagram for pions with PS coupling. We use the notation:

$$E_i^{(1)} = (\sqrt{s}/2) + p_0 - \rho_1 E_p, \quad E_f^{(1)} = (\sqrt{s}/2) + q_0 - \rho'_1 E_q,$$

$$E_i^{(2)} = (\sqrt{s}/2) - p_0 - \rho_2 E_p, \quad E_f^{(2)} = (\sqrt{s}/2) - q_0 - \rho'_2 E_q.$$

Here $\rho_i = \pm 1$ is the energy spin index of particle i , as indicated in Fig 2.

Form factor	Operator/ α	Effective operator/ α
D0	$(Q_1 - m)^{(1)}(P_2 - m)^{(2)}$	$E_f^{(1)} E_i^{(2)} O_4$
D11	$P_2^{(1)}(P_2 - m)^{(2)} + (Q_1 - m)^{(1)} P_2^{(2)}$	$[E_i^{(2)}(\sqrt{s} - E_i^{(1)} + E_f^{(1)}) O_4 + m E_f^{(1)} O_2 - m E_i^{(2)} O_3]$
D12	$Q_2^{(1)}(m - P_2)^{(2)} + (m - Q_1)^{(1)} Q_2^{(2)}$	$[E_i^{(2)}(E_f^{(1)} - \sqrt{s}) - E_f^{(1)} E_i^{(2)}] O_4 - m E_f^{(1)} O_2 + m E_i^{(2)} O_3$
D13	$P_1^{(1)}(P_2 - m)^{(2)} + (Q_1 - m)^{(1)} P_1^{(2)}$	$[E_i^{(1)} E_i^{(2)} + E_f^{(1)}(\sqrt{s} - E_i^{(2)})] O_4 - m E_f^{(1)} O_2 + m E_i^{(2)} O_3$
D21	$P_2^{(1)} P_2^{(2)}$	$-m^2 O_1 + m(\sqrt{s} - E_i^{(1)}) O_2 - m E_i^{(2)} O_3 + (\sqrt{s} - E_i^{(1)}) E_i^{(2)} O_4$
D22	$Q_2^{(1)} Q_2^{(2)}$	$-m^2 O_1 + m(\sqrt{s} - E_f^{(1)}) O_2 - m E_f^{(2)} O_3 + (\sqrt{s} - E_f^{(1)}) E_f^{(2)} O_4$
D23	$P_1^{(1)} P_1^{(2)}$	$-m^2 O_1 - m E_i^{(1)} O_2 + m(\sqrt{s} - E_i^{(2)}) O_3 + E_i^{(1)}(\sqrt{s} - E_i^{(2)}) O_4$
D24	$-P_2^{(1)} Q_2^{(2)} + Q_2^{(1)} P_2^{(2)}$	$2m^2 O_1 - m(2\sqrt{s} - E_i^{(1)} - E_f^{(1)}) O_2 + m(E_i^{(2)} + E_f^{(2)}) O_3$ $-[(\sqrt{s} - E_i^{(1)}) E_f^{(2)} + (\sqrt{s} - E_f^{(1)}) E_i^{(2)}] O_4$
D25	$P_2^{(1)} P_1^{(2)} + P_1^{(1)} P_2^{(2)}$	$2m^2 O_1 + m(2E_i^{(1)} - \sqrt{s}) O_2 + m(2E_i^{(2)} - \sqrt{s}) O_3$ $+[(\sqrt{s} - E_i^{(1)})(\sqrt{s} - E_i^{(2)}) + E_i^{(1)} E_i^{(2)}] O_4$
D26	$-Q_2^{(1)} P_1^{(2)} - P_1^{(1)} Q_2^{(2)}$	$-2m^2 O_1 + m(\sqrt{s} - E_f^{(1)} - E_i^{(1)}) O_2 + m(\sqrt{s} - E_i^{(2)} - E_f^{(2)}) O_3$ $-[(\sqrt{s} - E_i^{(2)})(\sqrt{s} - E_f^{(1)}) + E_i^{(1)} E_f^{(2)}] O_4$
D27	$-\gamma_\mu^{(1)} \gamma^{\mu(2)}$	$-O_5$

where the coefficients c_n are functions of the external momenta, the masses, and the energy spins of the initial and final states. Using the results in Table I we have

$$c_1 = m^2 [-D21 - D22 - D23$$

$$+ 2D24 + 2D25 - 2D26],$$

$$c_2 = m E_f^{(1)} [D11 - D12 - D13 - D22 + D24 - D26]$$

$$+ m E_i^{(1)} [-D21 - D23 + D24 + 2D25 - D26]$$

$$+ m \sqrt{s} [D21 + D22 - 2D24 - D25 + D26],$$

$$c_3 = m E_f^{(2)} [-D22 + D24 - D26]$$

$$+ m E_i^{(2)} [-D11 + D12 + D13 - D21 - D23$$

$$+ D24 + 2D25 - D26]$$

$$+ m \sqrt{s} [D23 - D25 + D26],$$

$$c_4 = E_i^{(2)} E_f^{(1)} [D0 + D11 + D12 - D13 + D24 - D26]$$

$$+ E_i^{(2)} E_i^{(1)} [-D11 + D13 - D21 - D23 + 2D25]$$

$$+ E_f^{(2)} E_f^{(1)} [-D12 - D22]$$

$$+ E_i^{(1)} E_f^{(2)} [D24 - D26]$$

$$+ \sqrt{s} E_i^{(1)} [D23 - D25] \quad (3.16)$$

$$+ \sqrt{s} E_i^{(2)} [D11 - D12 + D21 - D24$$

$$- D25 + D26]$$

$$+ \sqrt{s} E_f^{(1)} [D13 + D26]$$

$$+ \sqrt{s} E_f^{(2)} [D22 - D24]$$

$$+ s [D25 - D26],$$

$$c_5 = -D27.$$

The partial-wave decomposition^{8,11} can be done term by term. In the center-of-mass frame we introduce total and relative momenta

$$P_1 = \frac{P}{2} + p, \quad P_2 = \frac{P}{2} - p,$$

$$Q_1 = \frac{P}{2} + q, \quad Q_2 = \frac{P}{2} - q, \quad (3.17)$$

$$P = (\sqrt{s}, 0),$$

so that a general term in Eq. (3.15) reads

$$c_n(\sqrt{s}, p_0, q_0, \vec{p}, \vec{q}; \rho'_1 \rho'_2 \rho_1 \rho_2) \langle \vec{q}; \rho'_1 \rho'_2 \lambda'_1 \lambda'_2 | 0_n | \vec{p}; \rho_1 \rho_2 \lambda_1 \lambda_2 \rangle, \quad (3.18)$$

where ρ is the energy-spin index and λ the helicity. It is clear from (3.18) that in the Clebsch-Gordan algebra only the matrix elements of the operators introduced in (3.14) are needed since it involves only summations over the helicity index. Only one step, the integration over θ_{pq} , cannot be done analytically since the scalar form factors calculated by FORMF still depend on this angle.

We define

$$0_n(J; L'S'\rho', LS\rho; p, q, \theta) = \left[\frac{2L'+1}{2J+1} \right]^{1/2} \left[\frac{2L+1}{2J+1} \right]^{1/2} \\ \times \sum_{\lambda'\lambda} C_{0\lambda'\lambda'}^{L'S'J} C_{0\lambda\lambda}^{LSJ} d_{\lambda\lambda'}^J(\theta) \sum_{\substack{\lambda'_1\lambda'_2 \\ \lambda_1\lambda_2}} C_{\lambda'_1-\lambda'_2}^{1/2\ 1/2\ S'} C_{\lambda_1-\lambda_2}^{1/2\ 1/2\ S} \langle q, \theta, 0; \rho' \lambda'_1 \lambda'_2 | 0_n | p, 0, 0; \rho \lambda_1 \lambda_2 \rangle, \quad (3.19)$$

where ρ labels the four combinations of ρ_1 and ρ_2 . The partial-wave matrix element corresponding to the term (3.19) is then given by

$$pq \int d \cos \theta c_n(\sqrt{s}, p_0, q_0, p, q, \theta; \rho', \rho) 0_n(J; L'S'\rho', LS\rho; p, q, \theta). \quad (3.20)$$

The matrix elements (3.19) are evaluated with the algebraic program SCHOONSCHIP,¹² for the three different types of channels: singlet, uncoupled and coupled triplet, and arbitrary J . They are then combined into a FORTRAN subroutine which evaluates, given the coefficients c_n , the partial wave matrix elements (3.20).

In practice the coefficients c_n are also evaluated with SCHOONSCHIP, exactly as described in the example, since for the more complicated cases of pseudovector pion-nucleon coupling and of vector exchange it is very elaborate to calculate them by hand. The SCHOONSCHIP code performs the algebra by moving the P terms to their corresponding spinors, inserts the Dirac equation, and reduces the remaining operators to the standard form. A great advantage of the algebraic program is that the algorithm is the same for the crossed and the direct box, so once the algorithm is tested for the direct box it also works correctly for the crossed box of which we can only check some on-shell values given in the literature.^{4,13} Some extra complications encountered in the evaluation of the box diagrams for more general couplings are discussed in the Appendix. There we also give a discussion of the tests performed on the code.

In the remaining part of this section we discuss some symmetry properties of the kernel for the case of the BbS equation which reduce the number of coefficients c_n . In general one has to calculate 16 coefficients for each operator 0_n , but owing to the symmetry in p_0 and q_0 this number reduces to 10

for the BbS kernel. The partial-wave states introduced in Ref. 8 for the BSE are divided in states which are even in the relative energy p_0 and in states which are odd. In the BbS equation the relative energy is set equal to zero, which means that certain matrix elements of the kernel will vanish. For example, in the singlet NN channels we find

$$\langle {}^1J_f^+ | K | {}^3(J+1)_f^o \rangle = 0. \quad (3.21)$$

From this we deduce

$$\langle {}^1J_f^+ | K | {}^3(J+1)_f^e \rangle = \sqrt{2} \langle {}^1J_f^+ | K | {}^3(J+1)_f^{+-} \rangle. \quad (3.22)$$

Here e and o label the even and odd combinations of the ρ -spin states $(+ -)$ and $(- +)$. Working out all the combinations for every channel one can show that one only needs the coefficients c_n for (ρ_1, ρ_2) equals $(+, +)$, $(-, -)$, or $(+, -)$, in the initial and final state and with $(+ -)$ in the final and $(- +)$ in the initial state.

IV. CONSIDERATIONS AT THE ONE-LOOP LEVEL

Studies of the two-nucleon system with the BSE^{4,6} have indicated that the experimental phase shift parameters can better be described by a pseudovector theory for the pion-nucleon interaction than by a pseudoscalar theory due to the strong coupling between positive and negative-energy

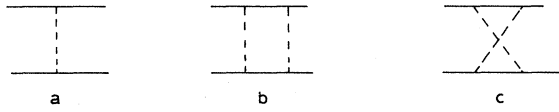


FIG. 3. The tree (a), the direct box (b), and the crossed box diagram (c).

states in the latter case. The possibility of a suppression of the negative-energy states by the crossed two-pion exchange contribution has sometimes been suggested.¹⁴ In this section we study this question in the one-loop approximation using a geometric unitarization of the nucleon-nucleon amplitude. In particular, the earlier calculations of Wortman¹⁵ and Haracz *et al.*¹⁶ for PS coupling are extended to the case of PV coupling.

The calculation is not complete, because we neglect the vertex and self-energy corrections. The diagrams considered here are shown in Fig. 3. The reason for not incorporating the vertex and self-energy corrections is that their contributions are expected to be small. Wortman found their effects for PS coupling “in the worst case for high energy and low partial waves” to be about 10% of the other fourth order amplitudes.¹⁵ We do not expect that these conclusions will be changed drastically for the case of PV coupling.

The calculation is similar to Wortman’s, we only use a different method to evaluate the amplitudes, i.e., as described in the previous section. Our calculations for PS coupling agree with those of Refs. 15 and 16 except for the lower partial waves. The differences are to be attributed to the high accuracy of our calculation of the box diagrams and to the omission of vertex correction and self-energy diagrams. The results are shown in Fig. 4. To get an idea of the relative importance of the crossed and the direct box we separately plotted the phaseshifts obtained from the tree diagram, the tree plus the direct-box diagram, and from all three diagrams in Fig. 3 both for PV and for PS coupling. The tree diagrams give the same result for PV and PS coupling, in view of the equivalence theorem.

In general the one-pion-exchange (OPE) diagram is not a good approximation, not even for the 3F_3 and 3F_4 partial waves. Adding the TPE box diagrams we find a much stronger effect in the PS case than in the PV case. We find, as was already observed by Wortman, that the box diagrams bring the OPE results closer to the data. It is certainly

not so that the crossed box always gives a much smaller contribution than the direct box. In some partial waves, e.g., 3P_2 , ϵ_2 , 1D_2 , 1F_3 (for PV), 3F_3 , and 3F_4 , the crossed-box contribution is larger than the one from the direct box.

For comparison the phase shifts have also been calculated, at the tree level, including all OBE diagrams, using the same coupling parameters as in the BSE given in Ref. 7. Together with the pion-box contributions they indicate that the PV coupling is preferred above the PS coupling in such a calculation. The large effects for PS coupling are due to the relatively strong coupling of positive and negative-energy states, as was also found in Refs. 1 and 4.

It has been conjectured by Müller and Glöckle^{17,18} that the BbS equation with a OBE kernel effectively sums all higher order diagrams and is in that respect superior to the BSE with the same kernel. The conjecture is based on model calculations with scalar particles. In our case, where the spin aspects have been incorporated in their full complexity, we do not find, at the one-loop level, any indication that the suggestion is valid.

In Tables II and III we compare the BbS and Gross approximation to the TPE direct-box diagram, for external on-mass-shell particles, with the exact value and also with the sum of the direct and crossed box diagrams. We find that neither of the approximations effectively sums the direct and the crossed box. They both represent a rather bad approximation to the direct box, and also significant differences exist between themselves, especially in the $^3(J-1)_J$ waves and in the singlet channels. Furthermore, from Table II we see that for PV coupling the crossed box dominates the direct box in the singlet and in the isospin 1 triplet channels, except in the $^3(J+1)_J$ waves. For PS coupling the situation is less clear; in general, the crossed box gives a contribution of the same order as the direct box and is negligible only in the 3D_1 channel. Moreover we see, as is to be expected, that the negative-energy states give a small contribution for PV coupling. They do not improve the approximation to the direct box. This is more strongly the case for PS coupling where we find that the inclusion of the negative-energy states increases the discrepancy between the exact and the approximated value. We therefore conclude that the negative-energy states are not correctly simulated by these quasipotential approximations. The same is found in Sec. V where we compare the solutions of the BbS equation to those of the BS equation.

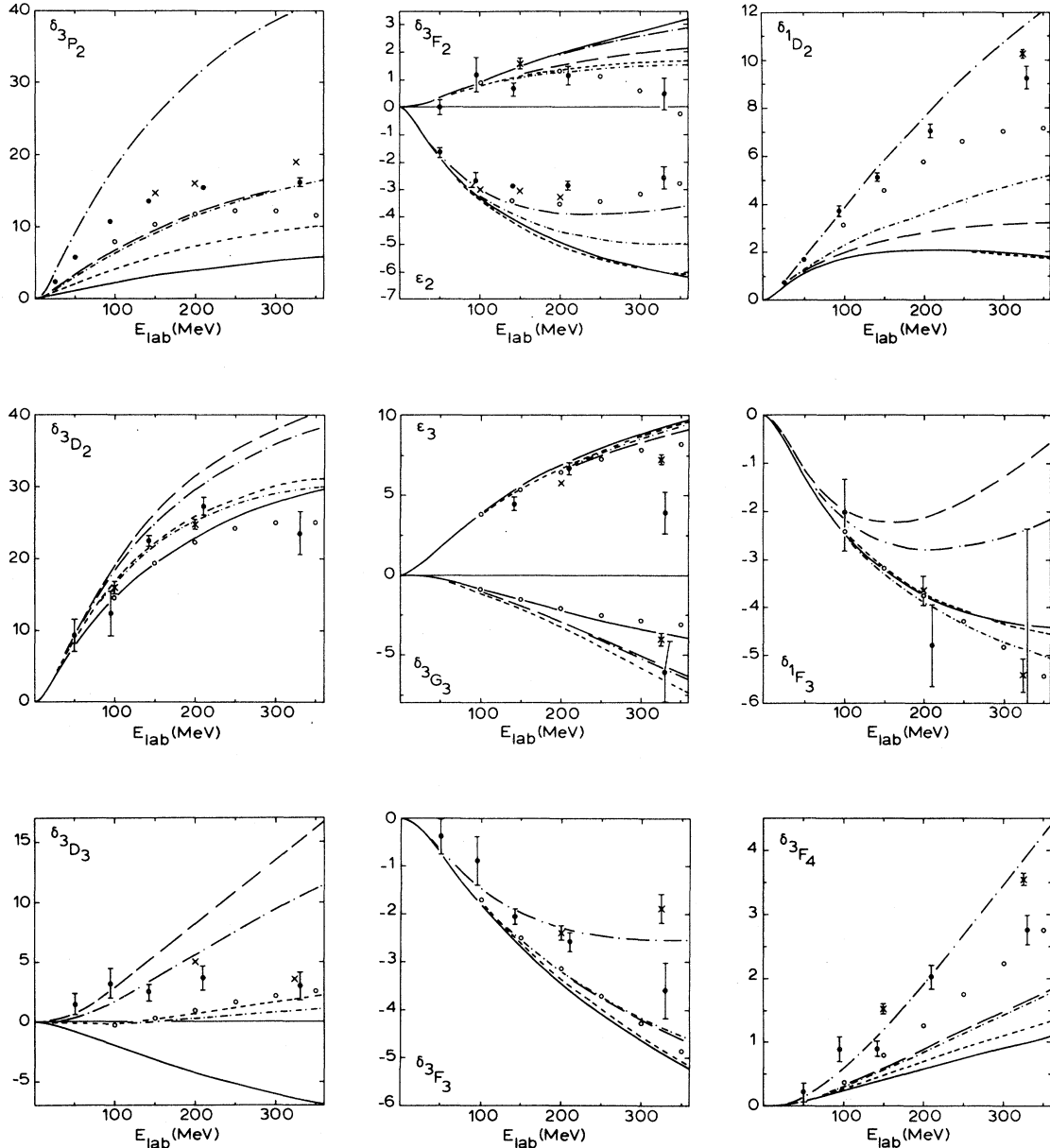


FIG. 4. The phase shifts calculated by geometric unitarization from the OPE (—), the OBE (○), OPE plus TPE direct box for PS coupling (—), PV coupling (— · — ·), the OPE plus TPE direct and crossed box for PS coupling (— · ·), and for the PV coupling (— · — ·). The data are the single energy fit of Ref. 19 (●) and Ref. 20 (○).

V. EFFECTS OF TWO-BOSON-EXCHANGE PROCESSES IN THE BbS EQUATION

Within the OBE approach one may examine how the solutions of the BbS equation compare with those of the BSE. The specific model adopted here is that of Refs. 4 and 6 with the BS coupling parameters for the OBE driving force given in

Table V. We consider two different situations. In the first case we use the BbS equation with all relevant intermediate states, as described in Sec. II. This will be called the six-channel calculation, although for $J \neq 0$ and uncoupled channels we have four and for $J=0$ we have only three intermediate states. In the second case we neglect the nonphysical channels in the intermediate states, i.e., we only

TABLE II. Comparison of the on-mass-shell TPE box diagrams in different approximations at 200 MeV for PV coupling. The first two columns give the OPE and OBE Born terms. For the OBE we use the BS parameters given in Table V. The next four columns give the direct box in BbS or Gross approximation with and without negative-energy states. The last two columns contain the exact values of the direct and the direct plus crossed boxes.

	OPE	OBE	2 ch BbS	6 ch BbS	2 ch Gross	4 ch Gross	D box	$D+X$ box
3S_1	-7.47×10^{-1}	-1.18	4.90	4.69	8.38	8.38	3.19	2.40
$^3S_1-^3D_1$	-5.61×10^{-1}	-2.22×10^{-1}	2.01×10^{-1}	1.90×10^{-1}	2.31×10^{-1}	2.30×10^{-1}	2.98×10^{-2}	6.77×10^{-2}
3D_1	-3.51×10^{-1}	-1.94×10^{-1}	-5.08×10^{-1}	-5.11×10^{-1}	-5.09×10^{-1}	-5.14×10^{-1}	-6.17×10^{-1}	-6.13×10^{-1}
1S_0	-7.47×10^{-1}	-1.71	8.14×10^{-1}	7.83×10^{-1}	1.23	1.22	4.99×10^{-1}	1.41
3P_0	7.47×10^{-1}	-2.97×10^{-1}	3.22×10^{-1}	3.11×10^{-1}	3.43×10^{-1}	3.24×10^{-1}	2.03×10^{-1}	1.19×10^{-1}
1P_1	-4.55×10^{-2}	-2.73×10^{-1}	1.19×10^{-1}	1.09×10^{-1}	4.04×10^{-1}	4.58×10^{-1}	2.77×10^{-2}	-8.37×10^{-2}
3P_1	-3.81×10^{-1}	-5.59×10^{-1}	6.39×10^{-2}	6.07×10^{-2}	7.76×10^{-2}	7.76×10^{-2}	3.54×10^{-2}	2.02×10^{-1}
3P_2	7.02×10^{-2}	2.07×10^{-1}	8.57×10^{-2}	8.62×10^{-2}	1.55×10^{-1}	1.55×10^{-1}	5.78×10^{-2}	1.32×10^{-1}
$^3P_2-^3F_2$	8.68×10^{-2}	6.32×10^{-2}	5.20×10^{-3}	5.07×10^{-3}	5.95×10^{-3}	5.91×10^{-3}	2.45×10^{-3}	-5.92×10^{-3}
3F_2	3.48×10^{-2}	2.40×10^{-2}	-8.13×10^{-3}	-8.16×10^{-3}	-8.25×10^{-3}	-8.30×10^{-3}	-1.02×10^{-2}	-1.12×10^{-2}
1D_2	3.61×10^{-2}	1.01×10^{-1}	5.41×10^{-4}	4.05×10^{-4}	2.69×10^{-3}	3.53×10^{-3}	-1.99×10^{-4}	2.75×10^{-2}
3D_2	4.23×10^{-1}	4.13×10^{-1}	9.94×10^{-2}	9.56×10^{-2}	1.10×10^{-1}	1.12×10^{-1}	6.18×10^{-2}	5.07×10^{-2}
3D_3	-7.45×10^{-2}	1.64×10^{-2}	1.20×10^{-1}	1.26×10^{-1}	2.07×10^{-1}	2.07×10^{-1}	8.57×10^{-2}	7.74×10^{-2}
$^3D_3-^3G_3$	-1.21×10^{-1}	-1.14×10^{-1}	8.44×10^{-3}	8.31×10^{-3}	9.68×10^{-3}	9.61×10^{-3}	4.29×10^{-3}	5.19×10^{-3}
3G_3	-3.95×10^{-2}	-3.56×10^{-2}	-1.32×10^{-2}	-1.32×10^{-2}	-1.34×10^{-2}	-1.35×10^{-2}	-1.72×10^{-2}	-1.71×10^{-2}
1F_3	-6.45×10^{-2}	-6.59×10^{-2}	1.34×10^{-3}	1.17×10^{-3}	2.64×10^{-3}	3.49×10^{-3}	2.57×10^{-4}	-2.83×10^{-3}
3F_3	-5.97×10^{-2}	-5.47×10^{-2}	2.01×10^{-3}	1.96×10^{-3}	2.12×10^{-3}	2.16×10^{-3}	1.26×10^{-3}	4.42×10^{-3}
3F_4	1.02×10^{-2}	2.18×10^{-2}	2.79×10^{-3}	2.76×10^{-3}	4.02×10^{-3}	4.02×10^{-3}	1.92×10^{-3}	4.51×10^{-3}
$^3F_4-^3H_4$	2.04×10^{-2}	2.01×10^{-2}	1.99×10^{-4}	1.97×10^{-4}	2.27×10^{-4}	2.54×10^{-4}	1.05×10^{-4}	-2.17×10^{-4}
3H_4	5.68×10^{-3}	5.80×10^{-3}	-3.32×10^{-4}	-3.33×10^{-4}	-3.37×10^{-4}	-3.39×10^{-4}	-4.34×10^{-4}	-4.61×10^{-4}
1G_4	1.26×10^{-2}	1.53×10^{-2}	5.61×10^{-5}	5.32×10^{-5}	6.66×10^{-5}	7.58×10^{-5}	2.32×10^{-5}	1.19×10^{-3}
3G_4	8.54×10^{-2}	8.68×10^{-2}	4.09×10^{-3}	4.03×10^{-3}	4.24×10^{-3}	4.28×10^{-3}	2.54×10^{-3}	2.12×10^{-3}

TABLE III. The TPE diagrams as in Table II for PS coupling. The first two columns have been omitted because they are identical for PS and PV coupling.

	2 ch BbS	6 ch BbS	2 ch Gross	4 ch Gross	D box	$D+X$ box
3S_1	2.92	-4.10×10^{-1}	3.93	-6.28	8.79	6.54
$^3S_1-^3D_1$	2.14×10^{-1}	2.63×10^{-1}	2.65×10^{-1}	3.42×10^{-1}	8.65×10^{-2}	1.43×10^{-1}
3D_1	-4.37×10^{-1}	-5.96×10^{-1}	-4.37×10^{-1}	-7.44×10^{-1}	-4.70×10^{-1}	-4.80×10^{-1}
1S_0	6.00×10^{-1}	2.67×10^{-1}	7.52×10^{-1}	-3.29×10^{-1}	1.16	4.31
3P_0	3.55×10^{-1}	2.67×10^{-1}	3.74×10^{-1}	1.88×10^{-1}	3.05×10^{-1}	1.58×10^{-1}
1P_1	2.18×10^{-2}	-7.82×10^{-1}	7.13×10^{-2}	-1.93	6.66×10^{-1}	3.91×10^{-1}
3P_1	7.41×10^{-2}	-2.49×10^{-2}	7.45×10^{-2}	-1.44×10^{-1}	1.11×10^{-1}	4.35×10^{-1}
3P_2	5.81×10^{-2}	-8.09×10^{-3}	8.10×10^{-2}	-1.26×10^{-1}	1.38×10^{-1}	5.33×10^{-2}
$^3P_2-^3F_2$	5.31×10^{-3}	5.92×10^{-3}	6.27×10^{-3}	7.24×10^{-3}	3.09×10^{-3}	-8.40×10^{-3}
3F_2	-6.90×10^{-3}	-1.05×10^{-2}	-6.99×10^{-3}	-1.39×10^{-2}	-6.83×10^{-3}	1.42×10^{-3}
1D_2	2.58×10^{-4}	-1.53×10^{-2}	3.33×10^{-4}	-3.74×10^{-2}	1.32×10^{-2}	9.73×10^{-2}
3D_2	1.15×10^{-1}	-2.92×10^{-2}	1.17×10^{-1}	-2.13×10^{-1}	1.88×10^{-1}	1.50×10^{-1}
3D_3	9.19×10^{-2}	-1.65×10^{-2}	1.25×10^{-1}	-1.95×10^{-1}	2.18×10^{-1}	1.72×10^{-1}
$^3D_3-^3G_3$	8.53×10^{-3}	9.24×10^{-3}	9.90×10^{-3}	1.10×10^{-2}	5.01×10^{-3}	6.14×10^{-3}
3G_3	-1.11×10^{-2}	-1.92×10^{-2}	-1.13×10^{-2}	-2.65×10^{-2}	-9.62×10^{-3}	-1.12×10^{-2}
1F_3	1.60×10^{-3}	-2.72×10^{-2}	1.49×10^{-3}	-6.51×10^{-2}	2.85×10^{-2}	1.71×10^{-2}
3F_3	2.28×10^{-3}	-9.47×10^{-2}	2.35×10^{-3}	-4.91×10^{-3}	4.47×10^{-3}	2.01×10^{-2}
3F_4	2.13×10^{-3}	-4.91×10^{-4}	2.78×10^{-3}	-4.35×10^{-3}	5.31×10^{-3}	2.32×10^{-2}
$^3F_4-^3H_4$	2.01×10^{-4}	2.14×10^{-4}	2.29×10^{-4}	2.47×10^{-4}	1.18×10^{-4}	-2.67×10^{-4}
3H_4	-2.78×10^{-4}	-5.38×10^{-4}	-2.82×10^{-4}	-7.54×10^{-4}	-2.03×10^{-4}	6.33×10^{-4}
1G_4	6.78×10^{-5}	-7.29×10^{-4}	6.52×10^{-5}	-1.69×10^{-3}	8.45×10^{-4}	5.71×10^{-3}
3G_4	4.53×10^{-3}	-2.69×10^{-3}	4.69×10^{-3}	-1.09×10^{-2}	1.00×10^{-2}	7.51×10^{-3}

consider those channels which exist on the (positive) mass shell. We call this the two-channel calculation. Unitarity is not affected by this approximation.

The results of the two calculations are shown in Fig. 5. The nonphysical channels are repulsive in all partial waves. They only give a significant contribution in the lower partial waves. The reason that their effect is small is due to the use of PV pion-nucleon coupling. In general we find that the six-channel calculation gives a better approximation to the BS phase shifts, although the improvement is often marginal. Only in the 1P_1 partial wave the disagreement with the BS results is greater by a small amount. A more detailed comparison of the negative-energy contributions calculated from the BSE with those from the BbS equation, given in Table IV, reveals that the latter in general overestimates the negative-energy states, especially in the lower partial waves. In the 1S_0 channel even the sign of the contribution is not correct, but also in the 3P_1 and 3D_2 partial waves we find relatively large deviations. The reason that the six-channel BbS equation seems to be a better approximation to the BSE is mainly due to the fact that the effects of the BbS approximation and of overestimating the negative-energy contributions tend to cancel each other. Since the effects of the negative-energy states are small, for PV coupling, it is tempting to incorporate them perturbatively into the kernel of

the QPE. This can be done by requiring that the one-loop diagrams are reproduced appropriately by the QPE.

The box diagrams are included as described in Sec. II of Ref. 1. The kernel W of the BbS equation

$$\phi = W - Wg_{\text{BbS}}\phi \quad (5.1)$$

is approximated by

$$W = K_{\text{OBE}} + X + D - D_{\text{BbS}}. \quad (5.2)$$

When K_{OBE} denotes the OBE kernel, X represents the crossed box diagrams of two-boson exchanges, and $D - D_{\text{BbS}}$ is the direct-box correction

$$K_{\text{OBE}}(S_{\text{BS}} - g_{\text{BbS}})K_{\text{OBE}}. \quad (5.3)$$

We first study the TPE contributions, which have the longest range. The agreement with the BSE is hardly improved by including the correction of the two-pion direct box into the driving force, as can be seen from Table IV. Only the 1S_0 , 3P_2 , and 3D_3 phase shifts are significantly improved, although this could just be accidental since the effects of other mesons, like the ω , are also significant. A remarkable point is that this correction leads to a distinctly lower 3D_1 phase shift as can also be seen in Fig. 5. In relation to this it is interesting to note that the ω contributions and the TPE crossed box have a negligible influence on this partial wave. The rather large effect of the TPE contribution in

TABLE IV. Comparison of the solution of the BS equation and the BbS equation at 200 MeV for PV coupling and BS parameters (Table V). The first four columns show the effects of the BbS approximation and the negative-energy states. The last four columns give the effects of the pion and omega box diagrams, in the two-channel approximation.

	BS 2 ch	BS 8 ch	BbS 2 ch	BbS 6 ch	BbS 2 ch π -D	BbS 2 ch $\pi + \omega$ -D	BbS 2 ch π -D + X	BbS 2 ch $\pi + \omega$ -D + X
1S_0	5.80	7.90	10.73	5.03	8.66	-8.99	31.09	16.97
3S_1	17.70	17.29	28.21	25.56	10.88	19.53	0.65	22.93
3D_1	-20.05	-20.08	-17.42	-17.65	-23.47	-24.07	-23.88	-23.98
ϵ_1	0.323	0.287	-1.64	-1.51	4.16	2.17	7.06	2.49
3P_0	1.09	-3.21	1.83	-2.48	-0.96	0.18	-4.34	-5.52
1P_1	-14.42	-14.83	-18.08	-18.55	-18.66	-14.31	-22.27	-23.12
3P_1	-20.66	-21.36	-19.98	-22.31	-20.69	-23.41	-16.63	-21.61
3P_2	13.68	12.66	14.42	12.81	12.11	9.65	17.23	13.56
3F_2	0.97	0.96	1.07	1.05	0.99	0.94	1.00	0.94
ϵ_2	-2.69	-2.68	-2.73	-2.70	-2.70	-3.14	-1.94	-2.47
1D_2	6.19	6.01	6.43	6.11	6.39	5.94	8.29	7.92
3D_2	25.95	24.38	29.11	26.46	25.64	26.54	24.73	25.23
3D_3	4.67	4.63	6.38	6.26	4.08	4.20	3.47	3.57

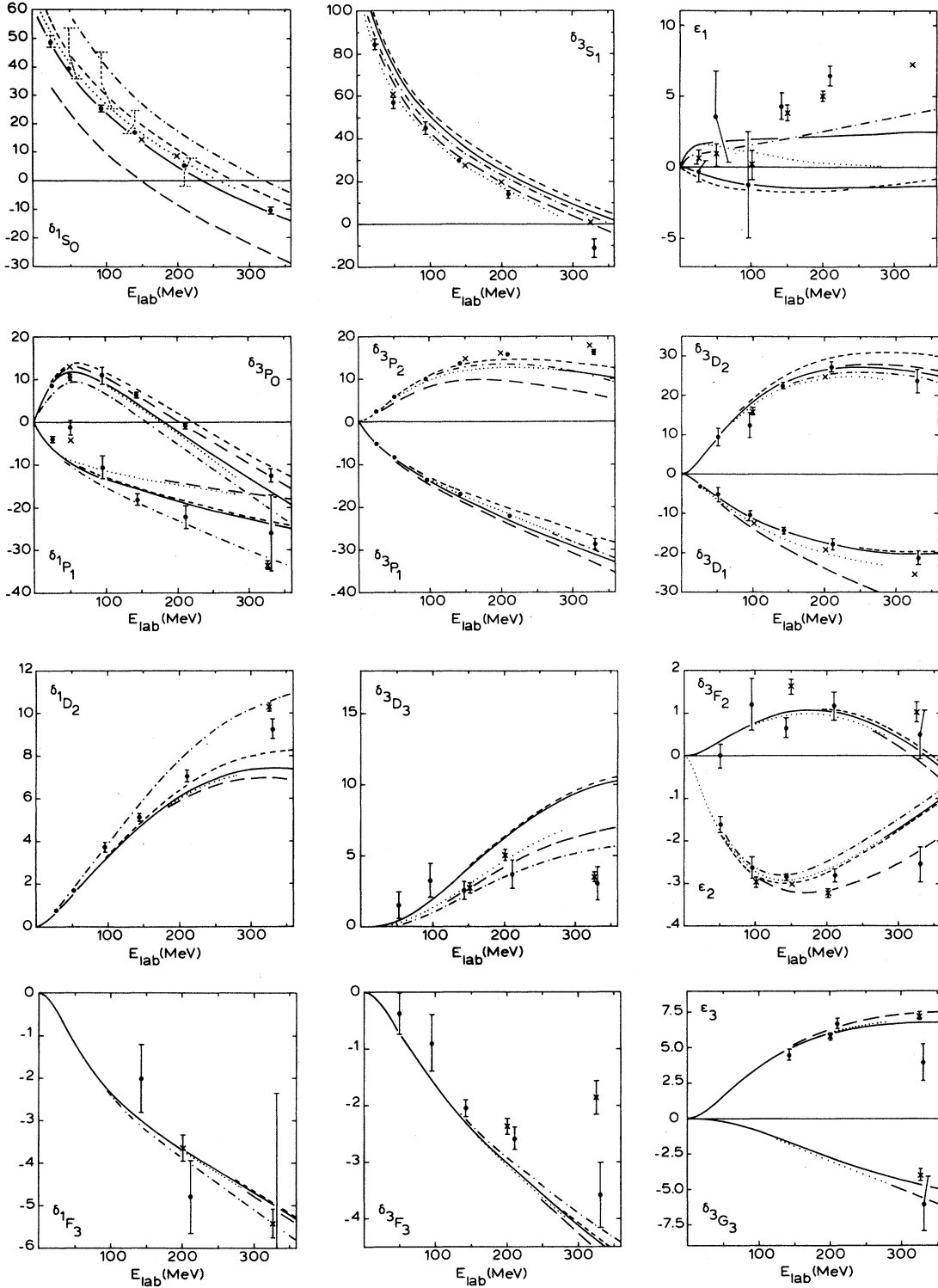


FIG. 5. The phase shifts of the BbS equation compared with those of the BSE (\cdots). The results are shown for the OBE kernel in the two-channel BbS equation ($---$) and in the six-channel equation ($---$). In the two-channel equation we also included the $\pi+\omega$ direct box correction ($---$) and the $\pi+\omega$ direct box correction plus the $\pi+\omega$ crossed box ($- \cdot - \cdot$). In the 3D_1 , 3F_2 , 3G_3 , and ϵ_3 channels the last two calculations give the same results on this scale.

the lower partial waves is due to the fact that the centrifugal barriers in these waves are low so that the short distance behavior is expected to be important. In particular, the ω -exchange contribution should play an important role in that region. The inversion of the S waves, caused by the TPE crossed box, is remedied by taking the ω into account, as can be seen from Table IV. In Fig. 5 the effect of the $\pi + \omega$ direct box is shown. This correction and all the following box contributions are calculated in the two-channel approximation. The influence of the $\pi + \omega$ crossed box is rather strong in the 1S_0 , 3P_0 , 1P_1 , 3P_2 , ϵ_2 , 1D_2 , and 3D_3 channels, but even in the F waves it is not negligible at higher energies. An important effect of the crossed box is the reduction of the $^1S_0 - ^3S_1$ splitting caused by the direct box correction. Furthermore, the extra repulsion in the 1P_1 and 3D_3 , and the attraction in the 3P_2 and 1D_2 can improve the OBE results. As was already inferred from the one-loop calculation there is in general no cancellation between the direct-box correction and the crossed box.

VI. FITS TO THE EXPERIMENTAL DATA

The inclusion of the TPE terms in the kernel of the BbS equation has the effect that the nucleon-nucleon phase shifts do not agree well any longer with the experimental ones. In the search for a new fit, starting from the results presented in Sec. V, we have neglected the S waves since they are affected strongly by the TPE terms and they are very sensitive to any short-range state-dependent force. A reasonable fit is found by changing $g_\omega^2/4\pi$ from 11 to 12 and by lowering $g_\rho^2/4\pi$ from 0.43 to 0.30. It turns out to be rather difficult to reduce the attrac-

tion in the 3P_1 and to lower the ϵ_2 without spoiling the other partial waves. The new coupling parameters are listed under fit B in Table V, where we also give the parameters for the fit of the two-channel BbS equation with the OBE kernel obtained in Ref. 6 for comparison, as fit A . The resulting phase shifts are plotted in Fig. 6. The introduction of the ω contributions in the box diagrams solves the problems for the 3P_1 and ϵ_2 , and in fact we obtain a qualitatively very nice fit when we neglect the S waves. The parameters for this fit are listed as fit C in Table V. In Sec. V we already observed that the inclusion of the ω meson in the box diagrams of the driving force greatly improves the S waves. In particular, the inversion of the 1S_0 and 3S_1 caused by the TPE terms is largely canceled. The same happens when we go from fit B to fit C . For example, fit B gives, at 100 MeV, 17.8° for the 3S_1 and 45.9° for the 1S_0 phase shift. These values are 48.6° and 35.3° , respectively, for fit C , which makes it feasible to obtain a fit including the S waves. To obtain the correct splitting of the 1S_0 and 3S_1 waves we have to lower g_ρ^V/g_ρ^T from 6.0 to 4.8. The value of $g_\epsilon^2/4\pi$ is obtained, as in Ref. 1, by fitting the binding energy of the deuteron. The resulting fit D is clearly somewhat too attractive in the S waves, and much too repulsive in the 3P_2 and 1D_2 channels. This can be cured by lowering the cutoff mass to 1.5. This is done in fit E , the other parameters are given in Table V. The fit in the 3P_0 and 1P_1 channels is now slightly worse but the 3P_2 , 1D_2 and the S waves are greatly improved. Also the ϵ_2 comes up too fast in this fit.

VII. CONCLUDING REMARKS

We have investigated the possibility of including the contributions of the direct and crossed box diagrams for nucleon-nucleon scattering within a quasipotential approach. These contributions are expected to play an important role in the nuclear force at intermediate distances. One particular way to account for the TPE diagrams is to calculate the one-loop corrections to the driving force in the QPE. However, in so doing we find that it is necessary to weaken in some way the short distance effects of these diagrams. This is done by including, in addition, the exchange of the ω mesons in the box diagrams. As a result a reasonable fit in all partial waves can be obtained.

An interesting conjecture has been made by Müller and Glöckle,¹⁷ that the BbS equation with

TABLE V. The coupling parameters for the various fits discussed in Sec. VI. For comparison we also give the BS parameters of Ref. 7. In all fits we have kept $g_\pi^2/4\pi=14.2$, $g_\delta^2/4\pi=0.33$, and $g_\eta^2/4\pi=3.09$.

Fit	$\frac{g_\epsilon^2}{4\pi}$	$\frac{g_\omega^2}{4\pi}$	$\frac{g_\rho^2}{4\pi}$	$\frac{g_\rho^T}{g_\rho^V}$	Λ^2
A	7.34	11.0	0.43	6.8	1.5
B	7.30	12.0	0.30	6.0	1.9
C	7.00	10.5	0.30	5.5	1.9
D	5.99	10.0	0.43	4.8	1.9
E	8.16	12.0	0.43	4.8	1.5
BS	7.30	11.0	0.43	6.0	1.9

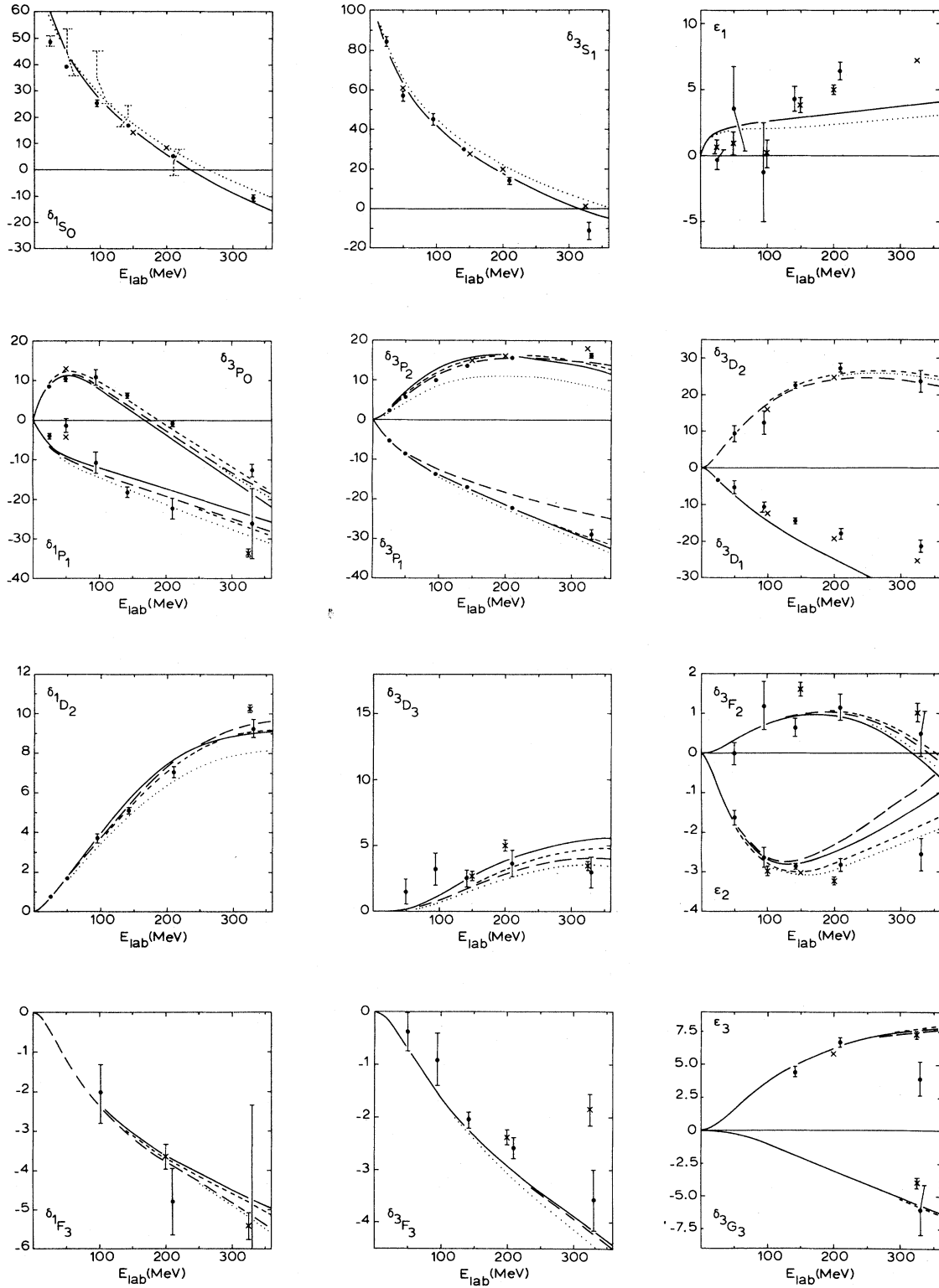


FIG. 6. The phase shifts for the fits discussed in Sec. VI. Fit B (—), fit C (---), fit D (···), and fit E (— · —).

one boson exchanges effectively sums all higher order diagrams. Although this conjecture has been verified for s waves in the case of scalar particles, no support for it has been found here. Owing to the complication of spin and isospin the cancellation between the one loop contributions does not take place in all channels. Furthermore, the possibility that the effects of negative energy states could appropriately be accounted for by introducing correction terms to the interaction in a quasipotential approach has been studied. Direct comparison of the results of both the BbS and Gross equations with the BS results indicates that in neither of them are the negative-state contributions represented well in this way.

Using the fits of the nucleon-nucleon phaseshifts obtained in Sec. VI, we may determine the deuteron wave function for such a model. However, in contrast to the Gross approach there are some conceptual problems with the definition of the deuteron current in the BbS model, as has been described in Ref. 21. There it is argued that the deuteron current cannot have the form of the impulse approximation, since it is then impossible to satisfy the BbS condition simultaneously for the final and the initial state. A further complication is that owing to the energy dependence of the driving force (when the box diagrams are included) it is necessary to introduce additional terms in the current operator. Clearly, it would be of interest to give a consistent treatment of both the two-nucleon system

and its electromagnetic properties in such a quasipotential approach.

ACKNOWLEDGMENTS

The authors would like to thank Prof. M. Veltman for making his program FORMF available to them. This work was supported in part by the Stichting voor Fundamenteel Onderzoek der Materie.

APPENDIX

In the actual evaluation of the box diagrams along the lines described in Sec. III some additional complications are encountered. The nominator of the expression (3.5) will contain higher powers of the loop momentum. This will force us either to use higher moments of the four-point function or to cancel these powers against factors in the denominator. We choose to cancel the powers of k against the nucleon propagators, leaving us with moments of the three- and two-point functions, which are expanded in terms of scalar form factors completely analogous to the four-point function. This procedure can be illustrated by looking at the same diagram as in Fig. 2, but now we take a pseudovector pion-nucleon coupling

$$\mathcal{L} = g_{PV} \bar{\psi} \gamma_\mu \gamma_5 \vec{\tau} \psi \cdot \partial^\mu \vec{\phi}. \quad (\text{A1})$$

The nominator of the integrand in Eq. (3.5) then reads

$$[k \gamma_5 (k + Q_1 + m) \gamma_5 (k + Q_1 - P_1)]^{(1)} [(k + P_2 - Q_2) \gamma_5 (k + P_2 + m) \gamma_5 k]^{(2)} \quad (\text{A2})$$

which can be written, after some straightforward algebra, as

$$[S_1^{-1} (P_1 - k + m) - (Q_1 + m)(k + Q_1 - m)(P_1 + m)]^{(1)} [S_2^{-1} (Q_2 - k + m) - (Q_2 + m)(P_2 - k - m)(P_2 + m)]^{(2)}. \quad (\text{A3})$$

S_1 and S_2 are the scalar parts of the propagators for nucleon one and two, respectively;

$$S_1 = \frac{1}{(k + Q_1)^2 - m^2} \text{ and } S_2 = \frac{1}{(k + P_2)^2 - m^2}. \quad (\text{A4})$$

The expression for the box diagram will now also contain the moments of the two- and three-point functions in Fig. 7.

A second complication is the use of strong form factors at the meson-nucleon vertices. They are, following the conventions of Ref. 6, of the monopole form

$$F(k) = \frac{\Lambda^2}{k^2 - \Lambda^2}, \quad (\text{A5})$$

where k is the momentum of the meson. For every meson line we thus have a factor

$$\frac{1}{k^2 - \mu^2} \left[\frac{\Lambda^2}{k^2 - \Lambda^2} \right]^2 = \frac{\Lambda^4}{\Lambda^2 - \mu^2} \left[\frac{1}{(k^2 - \Lambda^2)^2} - \frac{1}{\Lambda^2 - \mu^2} \left[\frac{1}{k^2 - \Lambda^2} - \frac{1}{k^2 - \mu^2} \right] \right]. \quad (\text{A6})$$

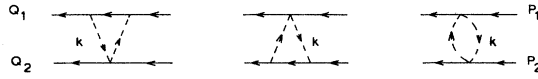


FIG. 7. The two- and three-point functions contributing to the crossed box diagram with PV pion-nucleon coupling.

This decomposition shows that we also have to know the form factors with quadratic meson propagators. Since these form factors are not provided by FORMF we calculate them numerically by taking the derivative with respect to the mass

$$\frac{1}{(k^2 - \Lambda^2)^2} = \frac{1}{2\epsilon} \left\{ \frac{1}{k^2 - \Lambda^2 - \epsilon} - \frac{1}{k^2 - \Lambda^2 + \epsilon} \right\} + O(\epsilon^2). \quad (\text{A7})$$

Here we gain an order ϵ in accuracy by shifting the two terms symmetrically with respect to Λ^2 . In practice this gain is limited by the accuracy of the form factors by FORMF, which is generally 10 to 12 digits. Only in certain situations, far from the mass shell, the program returns values with significantly less precision. Another source of inaccuracies is that $k^2 - \Lambda^2$ in Eq. (A7) can become much larger than unity. We then expand effectively in $\epsilon/k^2 - \Lambda^2$, which means that there is a large cancellation of significant digits in (A7). Since we also have to calculate form factors containing two quadratic propagators we will lose all accuracy in this

way. The optimal value of ϵ in such cases depends on the external momenta p and q and on their relative angle θ . In the program which calculates the box diagram ϵ is taken to be a function of p and q . The p - q plane is divided in regions with a fixed value of ϵ which is obtained from a stability analysis. It is found to be unnecessary to make ϵ a function of θ .

We now turn to the description of the tests of the numerical code. The partial wave routines were tested by evaluating the OBE matrix elements in this inefficient way and comparing them to the values obtained from the BS program of Fleischer and Tjon.⁶

Since FORMF also calculates the imaginary part of the diagrams we can check the imaginary part of the direct box, in the elastic region, since this can be calculated easily from the Born terms:

$$\begin{aligned} \text{Im}[D \text{ BOX}(p', p'_0, n'; p, p_0, n)] \\ = \frac{E}{2\hat{q}} \sum_m G(p', p'_0, n'; \hat{q}, 0, m) \\ \times G(\hat{q}, 0, m; p, p_0, n), \quad (\text{A8}) \end{aligned}$$

where G is the Born term, $\hat{q} = \sqrt{(s/4) - m^2}$ is the on shell momentum, and n indicates the partial wave channel.

Furthermore, we have compared the values of the direct box calculated by our program to the ones from the BS program. Finally, we reproduce the (on-shell) values of the various partial-wave matrix elements of the crossed box given in Refs. 4 and 13.

- ¹M. J. Zuilhof and J. A. Tjon, Phys. Rev. C **24**, 736 (1981).
- ²F. Gross, Phys. Rev. **186**, 1448 (1969).
- ³M. Glück, Phys. Rev. Lett. **28**, 1486 (1972); N. Dombey and B. J. Read, Nucl. Phys. **B60**, 65 (1973).
- ⁴J. Fleischer and J. A. Tjon, Phys. Rev. D **21**, 87 (1980).
- ⁵M. H. Partovi and E. H. Lomon, Phys. Rev. D **2**, 1999 (1970).
- ⁶J. Fleischer and J. A. Tjon, Nucl. Phys. **B84**, 375 (1975); Phys. Rev. D **15**, 2537 (1977).
- ⁷M. J. Zuilhof and J. A. Tjon, Phys. Rev. C **22**, 2369 (1980).
- ⁸J. J. Kubis, Phys. Rev. D **6**, 547 (1972).
- ⁹G. Passarino and M. Veltman, Nucl. Phys. **B160**, 151 (1979); G. 't Hooft and M. Veltman, *ibid.* **B153**, 365 (1979).
- ¹⁰M. Veltman, FORMF, a program for the numerical evaluation of form factors, Utrecht, 1979.
- ¹¹J. Fleischer, J. Comp. Phys. **12**, 112 (1973).
- ¹²M. Veltman, CERN report, 1967; H. Strubbe, Comp.

- Phys. Comm. **8**, 1 (1974); Comp. Phys. **18**, 1 (1979).
- ¹³J. Fleischer, J. L. Gammel, and M. T. Menzel, Phys. Rev. D **8**, 1546 (1973).
- ¹⁴G. E. Brown and A. D. Jackson, *The Nucleon-Nucleon Interaction* (North-Holland, Amsterdam, 1976), p. 107.
- ¹⁵W. R. Wortman, Phys. Rev. **176**, 1762 (1968).
- ¹⁶R. D. Haracz and R. D. Sharma, Phys. Rev. **176**, 2013 (1968); B. M. Barker and R. D. Haracz, *ibid.* **186**, 1624 (1969).
- ¹⁷L. Müller and W. Glöckle, Nucl. Phys. **B146**, 393 (1978).
- ¹⁸The cancellation of the 4th order diagrams in the limit $M_N \rightarrow \infty$ was already demonstrated by F. Gross, Phys. Rev. **186**, 1448 (1969).
- ¹⁹M. H. McGregor, R. A. Arndt, and R. M. Wright, Phys. Rev. **182**, 1714 (1969).
- ²⁰R. A. Arndt and B. J. Verwest, Department of Energy Report DOE/ER/05223-29.
- ²¹M. J. Zuilhof, thesis, University of Utrecht, 1981 (unpublished).